Int J Earth Sci (Geol Rundsch) (2017) 106:1133–1146
DOI 10.1007/s00531-016-1358-4

ORIGINAL PAPER

Structural context of the 2015 pair of Nepal earthquakes (Mw 7.8 and Mw 7.3): an analysis based on slip distribution, aftershock growth, and static stress changes

Revathy M. Parameswaran[1] · **Kusala Rajendran**[1]

Received: 10 January 2016 / Accepted: 14 June 2016 / Published online: 27 June 2016

Abstract The Great Himalayan earthquakes are believed to originate on the Main Himalayan Thrust, and their ruptures lead to deformation along the Main Frontal Thrust (MFT). The rupture of the April 25, 2015 (Mw 7.8), earthquake was east-directed, with no part relayed to the MFT. The aftershock distribution, coseismic elevation change of ~1 m inferred from the InSAR image, and the spatial correspondence of the subtle surface deformations with PT_2, a previously mapped out-of-sequence thrust, lead us to explore the role of structural heterogeneities in constraining the rupture progression. We used teleseismic moment inversion of P- and SH-waves, and Coulomb static stress changes to map the slip distribution, and growth of aftershock area, to understand their relation to the thrust systems. Most of the aftershocks were sourced outside the stress shadows (slip >1.65 m) of the April 25 earthquake. The May 12 (Mw 7.3) earthquake that sourced on a contiguous patch coincides with regions of increased stress change and therefore is the first known post-instrumentation example of a late, distant, and large triggered aftershock associated with any large earthquake in the Nepal Himalaya. The present study relates the slip, aftershock productivity, and triggering of unbroken stress barriers, to potential out-of-sequence thrusts, and suggests the role of stress transfer in generating large/great earthquakes.

Keywords Himalaya · Out-of-sequence thrusts · 2015 Nepal earthquakes · Large aftershocks · Coulomb stress changes · Stress heterogeneities

Introduction

The April 25, Mw 7.8 earthquake near Gorkha sourced ~80 km west-northwest of Kathmandu is the most recent event associated with the Himalaya convergence (Fig. 1a). Quite surprisingly, the earthquake was followed by a major aftershock on May 12 (Mw 7.3), located 75 km east-northeast of Kathmandu, which added to the huge damage already inflicted by the main shock. The central Himalaya, including parts of western and central Nepal, located between the rupture zones of the Mw 7.8, 1905 Kangra and Mw 8.2, 1934 Bihar earthquakes, is considered to be a seismic gap that holds potential to generate major earthquakes (Khattri 1987; Bilham et al. 2001; Rajendran et al. 2015). Thus, the April 25 event at the eastern end of the putative central seismic gap was not a surprise, but its large aftershock sourced ~140 km away from the main shock, a fortnight later, was unexpected since such delayed large aftershocks sourced on the fringes of the main shock rupture are rare (Henry and Das 2001; Elst and Shaw 2015). As for the Himalaya plate boundary, which has produced several large/great earthquakes, there are no known precedents for such occurrences during the modern-instrumentation period. The only exception from historic evidence is the Dehra Dun earthquake that occurred ~150 km away from the source location of the 1905 Kangra earthquake (Hough and Roger 2008). In this study, we begin by assuming that the second event (Mw 7.3) was an aftershock, since it falls within the rupture extent of the Mw 7.8 event that occurred 3 weeks prior to it. However, we redefine the later event

Electronic supplementary material The online version of this article (doi:10.1007/s00531-016-1358-4) contains supplementary material, which is available to authorized users.

✉ Kusala Rajendran
kusala@ceas.iisc.ernet.in

[1] Centre for Earth Sciences, Indian Institute of Science, Bangalore 560012, India

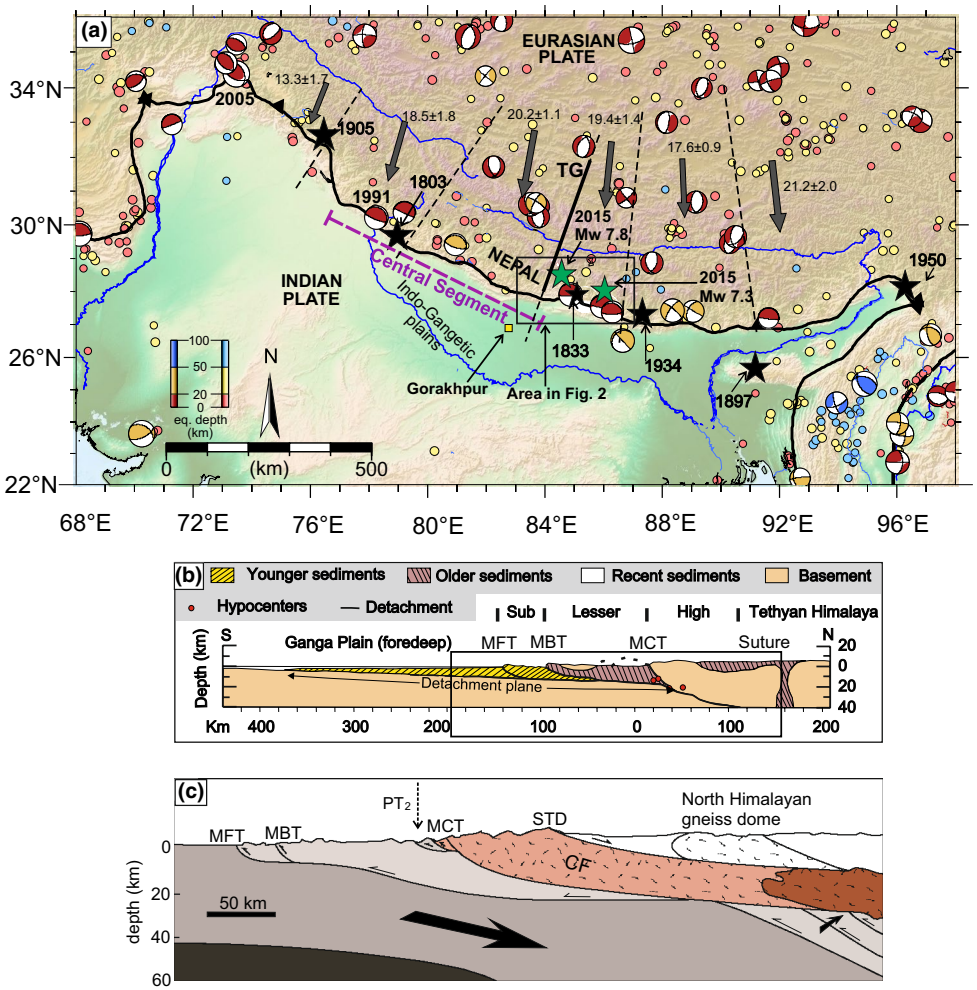

Fig. 1 Map showing large and great earthquakes in the Himalaya (1991 Uttarkashi has Mw < 7; however, it is discussed in the text). **a** *Black stars* historical events (Mw ≥ 8): A.D., 1897, 1905, 1934, 1950. Other significant large earthquakes: A.D., 1803, 1833, 2005 events. *Green stars* 2015, Mw 7.8 and Mw 7.3 earthquakes. *Colored circles* background seismicity; 1977 present (6.5 > Mw ≥ 4.5). *Colored beachballs* focal mechanisms of events with 8 > Mw ≥ 6.5. *Gray arrows* GPS convergence rates in mm/yr (after Stevens and Avouac 2015). TG: location of Thakkola Graben marked by *solid line* (after Ader et al. 2012). **b** Generalized cross section of the central Himalaya showing the Main Central Thrust (MCT), the Main Boundary Thrust (MBT), and the Main Frontal Thrust (MFT). Detachment plane coincides with the Main Himalayan Thrust (MHT). **c** *Rectangular* region from (**b**); CF is channel flow (after Hodges 2006); MFT, MBT, MCT are the same as in Fig. 1b (after Rajendran et al. 2015). South Tibetan Detachment (STD)

as a triggered aftershock based on results reported in this paper. That both these earthquakes did not cause any serious damage in the northern Indian plains was also surprising because it is contradictory to the general perception that rupture from large central Himalayan earthquakes is likely to propagate southward (e.g., Mw 8.2, 1934 Bihar–Nepal earthquake). Damage from the main shock was mostly confined to the Kathmandu Valley with minimal effects in the northern Indian plains, and unlike the 1934 event, it did not cause any liquefaction in the north Indian plains, suggesting low shaking effects in these regions (Parameswaran et al. 2015).

Large earthquakes are believed to originate on the Main Himalayan Thrust (MHT), the décollement, along which the northern fringe of the Indian plate underthrusts the Himalaya at a rate of approximately 20 mm/yr (Lavé and Avouac 2000; Fig. 1b). Prevailing models suggest that the consequent slip is relayed to the southern, younger thrust fault systems, and thus the ruptures of MHT earthquakes are expected to emerge at the Main Frontal Thrust (MFT) (Seeber and Armbruster 1981). However, as the fault-propagation folding absorbs much of the slip, evidences for surface slip are subtle or nonexistent (Yeats and Lillie 1991). The proposed mechanism of southward transmission of slip is validated by trenching observations in the foothills of the Himalaya that have exposed fault offsets from the 1934 and older events (Sapkota et al. 2013; Rajendran et al. 2015). There are also other modes of slip as observed in the case of the Mw 7.6, 2005 Kashmir earthquake that produced a ~70-km-long primary surface rupture, with a maximum vertical offset of 7 m (Kaneda et al. 2008). However, it may be noted that this earthquake was sourced on the morphologically conspicuous, Balakot-Bagh fault in the sub-Himalaya, tangential to the MBT, and is considered quite different from a typical décollement earthquake (Kaneda et al. 2008). Hussain and Yeats (2009) interpret that the Balakot-Bagh fault is in fact a part of the Indus-Kohistan Seismic Zone (IKSZ), a reverse-faulting region extending from ~72.5°E to ~74°E paralleling the MBT in a NW–SE direction, as reported by Armbruster et al. (1978). Another notable earthquake is the Mw 7.0, 1991 Uttarkashi earthquake that presumably originated on the MHT, but its rupture was modeled as arrested at the base of the crustal ramp (Cotton et al. 1996).

Based on field observations and source models, most researchers have ruled out propagation of the 2015 rupture to the MFT, and assign much of the slip to the MHT, the detachment plane to which the former soles into (Goda et al. 2015; Parameswaran et al. 2015; Avouac et al. 2015; Fan and Shearer 2015; Yagi and Okuwaki 2015; Hayes et al. 2015). Most field surveys also rule out the possibility for any potential surface rupture, with the exception of Parameswaran et al. (2015) who reported ground cracks/fractures, located to the south of a physiographic transition and out-of-sequence thrust (PT_2), discussed widely in the literature (Fig. 1c; Wobus et al. 2006b; Hodges 2006). Subtle, but spatially consistent with the coseismic deformation observed on the InSAR imagery (Lindsey et al. 2015), these surface breaks were interpreted as evidence for the potential role of such thrust systems in accommodating slip from earthquakes on the MHT. This event is the first large modern-day earthquake in the central Himalaya, which unlike its 1934 predecessor, terminated ~50 km north of the MFT (Angster et al. 2015). The 2015, Mw 7.8 event shows striking resemblance to the 1833 earthquake, an M 7.6 event that struck ~100 km ESE of its epicenter, in terms of damage and occurrence of a blind rupture (Grandin et al. 2015). Although not within the same section of Himalaya, the 1905, Mw 7.8 earthquake did not propagate beyond the Jwalamukhi fault (Hough and Roger 2008), similar to the style observed in the 2015 earthquake.

There are no other modern-day large earthquakes sourced in the Nepal Himalaya to suggest whether their rupture mechanisms are different from its historical and recent precedents (e.g., 1934 Bihar–Nepal, 1991 Uttarkashi, 2005 Kashmir). While several notable recent works have produced reasonably concurring models on the 2015 earthquake (Avouac et al. 2015; Fan and Shearer 2015; Yagi and Okuwaki 2015; Hayes et al. 2015), there remains a lack of accord on the associated structures. In particular, there is no consensus on the role of heterogeneities in controlling the rupture. In this paper, we present slip models, static stress changes, growth of aftershock area, and surface deformation of the 2015 events, to comment on the potential role of structural heterogeneities in the rupture process and its relation with the regional morphotectonic framework. Here we start with a brief summary of the seismotectonic setting of central Nepal Himalaya and discuss the source characteristics of the April–May pair of earthquakes.

Seismotectonics of Nepal Himalaya

The central Nepal Himalaya is considered as a classic example of continent–continent collision, where the underthrusting of Indian Plate has occurred along several, roughly east–west-trending fault zones, within a ~100-km-wide belt (Le Fort 1975; Hodges et al. 2001). The general structure of the Himalaya collision zone is defined by a series of gentle, north-dipping, thrust faults that grow progressively younger southward (Fig. 1a, b). The oldest and the northernmost is the Main Central Thrust (MCT), which formed ~24–21 Ma ago. This is followed by the Main Boundary Thrust (MBT), believed to have been active until ~5 Ma ago, and the youngest and southernmost, the ~2 Ma, Main Frontal Thrust that shows continuing deformation (MFT) (Lavé and Avouac 2000; DeCelles et al. 2001). Both MCT and MBT sole into the Main Himalayan Thrust (MHT), the active parts of which are estimated to absorb 19 ± 2.5 to ~21 mm/yr of shortening (Bettinelli et al. 2006; Lavé and Avouac 2000).

North of the active collision boundary, this segment of the Nepal Himalaya accommodates significant crustal shortening and uplift on the MHT ramp, giving rise to several spectacular orogenic landforms. For example, some of the tallest peaks such as the Annapurna and Mt. Everest, ~20 km north of the MCT, are located in this segment. Recent estimates of convergence rates suggest lateral variations along the strike of the Himalaya, from 13.3 ± 1.7 to 18.5 ± 1.8 mm/yr eastward in the western Himalaya (Ader et al. 2012; Stevens and Avouac 2015). Further east, convergence rate increases to 20.2 ± 1.1 mm/yr, followed by a drop to 19.4 ± 1.4 mm/yr, and between ~86.5°E and 91.5°E it drops further to 17.6 ± 0.9 mm/yr (Fig. 1a). Such variations have perhaps controlled the geomorphologic evolution, as evidenced by the presence of the Thakkhola Graben (TG) in the eastern Nepal that has developed between two segments with different convergence rates (Ader et al. 2012). An alternate explanation for the formation of TG is the E–W extension similar to that seen in Tibetan region as evidenced by great strike-slip earthquakes such as the M 8 1951 Beng Co event (Armijo et al. 1989).

The geometry of the thrust system, and the evidence for recent surface faulting events observed along the trace of the MFT would suggest larger uplift rates in the lower Himalaya compared to that in the higher Himalaya. However, it has been observed that the highest peaks are not within the MFT, but are located 100–150 km to its north (Lavé and Avouac 2000). Some authors attribute such drastic changes in physiography and higher uplift rates to the presence of a mid-crustal ramp in the MHT (e.g., Cattin and Avouac 2000). Existence of a crustal ramp is supported also by the pattern of microseismicity recorded by a 5-station network (Pandey et al. 1999) as well as the Himalayan Nepal Tibet Seismic Experiment (HIMNT) (Monsalve et al. 2008). Nábelek et al. (2009) sites the presence of a low-velocity zone beneath Nepal Himalaya which they ascribe to the underthrusting of a shallow MHT underneath the Gangetic sediments in the Lesser Himalaya and the consequent release of water. A ~250-km-long, arcuate

patch of strike-slip earthquakes sourced at 60–100 km depth, located south of the Tibetan plateau, between 86°E and 88°E longitude (de la Torre et al. 2007) is perhaps a unique aspect of the seismicity of eastern Nepal. Rajendran et al. (2011) consider this as an evidence for extension due to slab pull within the leading edge of the subducting plate, citing the example of the Mw 6.9, 2011 Sikkim event, the most recent and the largest to fall in this category of deep-crustal, upper-mantle, strike-slip earthquakes to have occurred here.

Although the MCT is considered mostly inactive, some studies suggest its recent reactivation including a major displacement around ~5.5 Ma in the Nepal Himalaya (Seeber and Gornitz 1983; Hodges et al. 1996). More recent studies based on stream-profile analysis and 40Ar/39Ar thermochronology have led to the identification of a prominent physiographic break named PT_2, which some researchers consider as an out-of-sequence thrust that separates the southern regions of moderate elevation from those of higher elevations in the north (Burbank et al. 2003; Wobus et al. 2003, 2006a, b; Hodges et al. 2004). Located within a few tens of kilometers south of the MCT, these workers consider this structure a zone of active uplift and erosion (Fig. 1c). Studies have also linked the high uplift rates to channel flow and ductile extrusion from the Southern Tibetan plateau, leading to accelerated surface denudation focused along the southern margins of the MCT (Beaumont et al. 2001; Hodges 2006). The sequential reorganization of drainage pattern reported in the southern Tibet (Clark et al. 2004) and the eclogite formation on Kakhtang thrust in Bhutan attributed to pulsed-channel flow (Hollister and Grujic 2006) are also supportive of the extrusion theory. However, the existence of channel flow remains debated and at this point and we restrict our discussion to the physiographic break as related to an out-of-sequence thrust.

Aside from the out-of-sequence thrust theory, the steepness of the ranges in the higher Himalaya is attributed to the growth of duplex zones. This region of the Himalaya is believed to have undergone continuous growth over the past 10 Myr, primarily due to the underplating, following the growth of duplex zones in the Lesser Himalaya (Herman et al. 2010). The few crustal images available for these regions based on the HIMNT data suggest relatively low V_P/V_S ratio at depths from the surface to 40 km below the sea level for regions located north of latitude 27.5°N (Monsalve et al. 2008). Finer imagery of the geometry of the duplex zones, higher resolution of the velocity anomalies, and further confirmation on the presence or absence of channel flow is possible only with more geophysical modeling of the region. Admittedly, there are limitations for seismotectonic interpretations, as observed for the 2015 pair of Nepal earthquakes, until such finer images are available.

Definition of the problem

Previous studies have attempted source models, rupture directivity, InSAR-based deformation, synthesis of aftershock data, and other studies provide considerable information about the 2015 earthquakes. For example, backprojection models of high- and low-frequency P-waves by Fan and Shearer (2015) suggested a multiple asperity model and a complex three-stage rupture process. Rupture complexity was implied also by Avouac et al. (2015), who used teleseismic records and SAR data to suggest a ~140-km-long eastward rupture possibly arrested by a zone of lower stress or a rate-strengthening patch of the MHT. On the other hand, the hybrid backprojection model by Yagi and Okuwaki (2015) suggested an irregular deceleration of rupture before it arrested at its eastern limit, which they attributed to heterogeneity in the stress drop. Based on in-depth finite fault modeling using teleseismic and geodetic data, and careful analysis of previous events, Hayes et al. (2015) conclude that this segment of the Nepal Himalaya is quite distinct in seismicity and source mechanism.

The aftershock that occurred 17 days later and located ~140 km away from the main shock is the first post-instrumentation example of its kind in the Nepal Himalaya. In fact, the aftershock was sourced close to the zone of initial rupture arrest, and the subsequent shocks formed a tight spatial cluster west of 86.5°E (Fig. 2). Adhikari et al. (2015) used ~3000 aftershocks spanning over the first 45 days to suggest that the rupture was centered on the Kathmandu klippé, in line with previous suggestions on the role of mid-crustal ramps in localizing seismicity (e.g., Pandey et al. 1999). These authors also suggest that the Mw 7.8 event may have ruptured the region broken by a previous event of similar magnitude (1833, M 7.6). It is quite possible that this segment of Nepal Himalaya exhibits a distinctive rupture style, and it might or might not have mimicked the 1833 rupture (Martin et al. 2015). Given the incompleteness of historic evidence, it is premature to conclude whether the 2015 rupture overlaps with that of 1833.

In light of previous studies which have used a variety of data and methods, it is clear that the April 2015 rupture originated on the MHT, propagated eastward, without moving up-dip to the MFT. Therefore, most of the slip remains confined to the Kathmandu region, and left the Indo-Gangetic plains in the south relatively unaffected. It has also been noted in these works that heterogeneities in the area of rupture may have played a considerable role in controlling the path and magnitude of the rupture, and relayed stresses to regions south of the fault plane. It is, however, still unclear (1) what caused the along-strike termination of the rupture and aftershocks, (2) what is the nature of the heterogeneity, if any, that could have caused these abrupt terminations, and (3) how the static stress has changed in

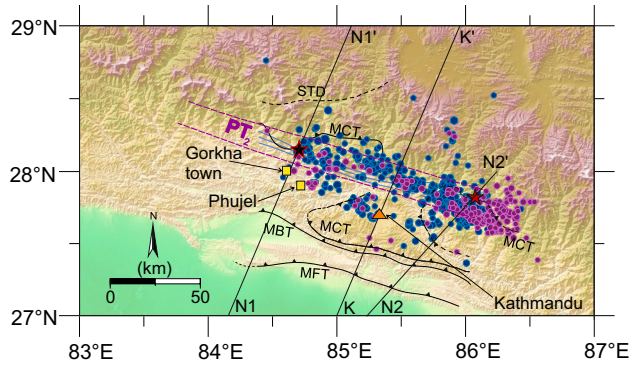

Fig. 2 Map of eastern Nepal region showing the epicenters of the main event and its aftershocks. *Black star* epicenter of April 25, Mw 7.8; circles filled in shades of *blue* are its aftershocks that are defined by temporal and spatial proximity. *Red star* May 12, Mw 7.3; *circles filled* in *purple* are its aftershocks. N1–N1′ is a cross section through the Mw 7.8 epicenter and K–K′ is a cross section through Kathmandu; both perpendicular to the strike of the main event. N2–N2′ is a cross section through Mw 7.3 epicenter, perpendicular to the strike of its fault plane. Thrust belts after Wobus et al. (2006b). PT2 zone is marked after Parameswaran et al. (2015) and Wobus et al. (2006b). Cross sections are discussed in detail in Fig. 6

the surrounding regions. This paper explores possible structural controls hosted within the Nepal Himalaya that could address some of these issues.

Methodology

This study uses aftershock data, slip distribution, and Coulomb static stress changes to understand the source characteristics of the 2015 pair of Nepal earthquakes, in particular the relation between the two events and their connection to the regional tectonics. We use the aftershock data to map the spatial and temporal growth, with respect to the slip and stress distributions. To compute the slip, we use moment inversion of teleseismic body waves (Kikuchi and Kanamori 1991, 2003). Some recent papers have discussed source models that provide estimates of slip distribution and their temporal growth within the rupture zone (e.g., Avouac et al. 2015; Fan and Shearer 2015; Yagi and Okuwaki 2015; Hayes et al. 2015). These studies suggest the potential role of multiple asperities in the spatio-temporal growth of slip. Our source models for the two earthquakes are similar to previous studies in terms of both magnitude and distribution of slip, and here we use them to explore any possible structural connection with the purported out-of-sequence thrusting. We use Coulomb static stress changes induced by the April 25 event (Coulomb 3.0, USGS) to explain the large aftershock on May 12. Published schematic models for Nepal Himalaya (e.g., Hodges 2006; Wobus et al. 2006a, b) provide the basic framework for the 2-D projections of slip along the various transects (Fig. 2).

Aftershock data

For the purposes of this study, we have used the aftershock data from Adhikari et al. (2015). We use 553 well-located aftershocks of magnitude $M_L \geq 4$ and depth <60 km, collected by the National Seismological Centre, Nepal, over a period of 45 days after the mainshock. The events show an abrupt termination ~86.5°E, which at the outset suggest a structural control (Fig. 2). Three transects were taken through the region of aftershocks to analyze their depth distribution along selected profiles. Of the three profiles N1–N1′ and K–K′ are perpendicular to the general structural trend (~strike 293°), the former cutting through the source zone of the Mw 7.8 event, and the latter through the Kathmandu basin. A third profile N2–N2′ that traverses the aftershock zone of the Mw 7.3 event is not exactly perpendicular to the structural trend, but has a different strike of 312°, made to coincide with the strike of the fault plane of the May 12 earthquake (Fig. 2). These transects are discussed in detail later.

Moment inversion using teleseismic body waves

Waveform data for moment inversion of the April 25, 2015, Mw 7.8 event was obtained using Wilber-3 tool from the Incorporated Research Institutions for Seismology-Data Management Centre (IRIS-DMC) database, for both P- and SH-waves. We used 34 P-waves and 6 SH-waves, from 36 Global Seismic Network (GSN) broadband stations (Fig. fs1; fs – figures in supplementary material). The first 100 s of P- and SH-waves were chosen from epicentral ranges of 30°–90° and 30°–70°, respectively, to avoid PP, SS, and SKS contamination. A high-pass filter of 0.002 Hz was used to remove long-period waves that could have been generated during the integration step to convert the signals from velocity to displacement. A low-pass filter of 1 Hz was used to remove high-frequency signals generated due to the interaction of seismic waves with surface complexities. P- and SH-waves for the first 100 s were inverted for a fault plane area of 160 × 138 km^2 that approximately defined the zone of aftershocks from April 25 to May 30, 2015. The hypocenter was placed at a depth of 15 km, compatible with other source models (USGS; Avouac et al. 2015; Fan and Shearer 2015). Strike (293°), dip (7°), and rake (108°) of the fault plane were based on the Harvard GCMT solution. A best-fit rupture velocity of 2.75 km/s in combination with the velocity model obtained from Crust 2.0 (Bassin et al. 2000) was used. Moment release was computed using four triangular time functions with half-base lengths set as 2.5 s. The resulting focal mechanism,

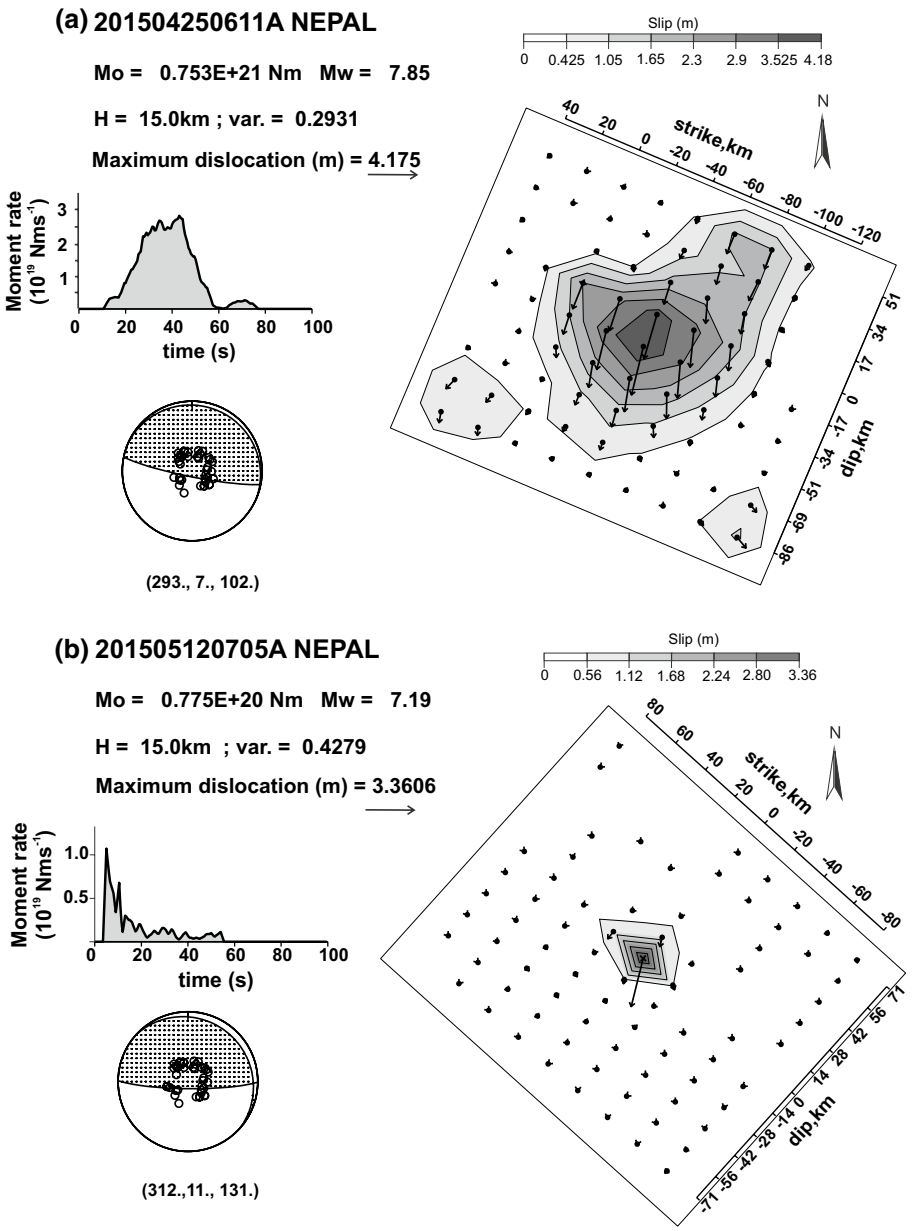

Fig. 3 Moment release, focal mechanism, and slip distribution: **a** the April 25 and **b** the May 12 events

source parameters, and the slip distribution are discussed later (Fig. 3a).

Similar procedure was followed for the May 12 earthquake that occurred ~140 km east of the main shock, and a similar number of waveforms were used from 34 broadband GSN stations (Fig. fs2). Aftershocks from May 12 to May 30, 2015, were used to define the initial bounds of the fault plane, and a final area of 160 × 142 km^2 provided the best results. Hypocentral depth of 15 km and fault parameters (strike 312°, dip 11°; rake 127°) were based on the Harvard GCMT solution. The resulting focal mechanism, source parameters, and the slip distribution are discussed later (Fig. 3b). As the strike and dip of our solutions are consistent with that of the Harvard GCMT and only the rake differs, we have used the latter for Coulomb static stress change calculations.

Coulomb static stress change

Computation of Coulomb static stress changes due to an earthquake depends on the choice of receiver fault planes. In this work, the Coulomb static stress change due to the Mw 7.8 earthquake is computed for different sets of receiver fault planes at varying depths. We examine the spatial connection of the major aftershock on May 12, with regard to the stress changes caused by the main shock. Based on the Harvard GCMT solution, the source mechanism of this aftershock is very similar to that of the main

shock, which suggests that the causative faults share similar geometry. But, since the source of the Mw 7.3 aftershock that occurred more than a fortnight later is located at the terminus of the initial rupture there is a question whether it was sourced on the fringes of the main slip or on an adjoining patch of high stress. We used the subfault data from USGS to compute the static stress change due to the April 25 earthquake with respect to receiver faults identical to the main rupture (strike 293°, dip 7°, and rake 108°) at different depths (Fig. 4a–c) for an effective coefficient of friction $\mu = 0.40$. Similarly, stress changes were computed for receiver faults of strike 312°, dip 11°, and rake 127°, representing the causative fault of the May 12 event (Fig. 4d).

Results

The moment inversion for the first event results in a solution of Mw 7.85 and a pure thrust focal mechanism on a fault plane with strike 293°, dip 7°, and rake 103° (Fig. 3a; Fig. fs3). The net moment release of 0.753E + 21 Nm occurs over a total period of 70–80 s, with a uniform, Gaussian distribution for the first ~50 s, after which the release is rather small compared to the maximum moment release. The maximum dislocation is found to be 4.17 m, ~40 km southeast of the epicenter, and the average slip is 0.1003 m distributed within 160 × 138 km^2 of the fault area. The slip vectors are directed up-dip, typical of thrust faults. The basic elements of our solution are compatible with those obtained by Avouac et al. (2015), Fan and Shearer (2015), Yagi and Okuwaki (2015), and Hayes et al. (2015) (Table 1). The up-dip end of the fault plane that extends toward the Indo-Gangetic plains shows minimal slip in all these models, explaining the nominal surface deformation observed in the field (Parameswaran et al., 2015). Compatibility of slip models by various groups, although using different sets of data and techniques, gives us confidence to use our slip model for further discussions on the tectonic and morphologic effects of the earthquakes.

The solution for the second event also shows a pure thrust mechanism on a fault plane of strike 312°, dip 11°, and rake 131° (Fig. 3b; Fig. fs4). A magnitude of Mw 7.19 was obtained with a net moment of 0.775E + 20 Nm, released in just over ~50 s. However, unlike the main shock, most energy from this earthquake seems to have been released within the first ~10 s of the rupture. The slip distribution is also highly localized (40 × 28 km^2) around the source, with maximum up-dip slip of 3.36 m.

Coulomb static stress changes due to the Mw 7.8 event show complex patterns. However, computation carried out depth-wise validates an expected result. Figure 4a–c shows the Coulomb static stress change due to the main shock with respect to receiver faults of strike 293°, dip 7°, and rake 108° at depths of 5, 7, and 15 km, respectively. It is clear that the static stress change increases up-dip of the main fault implying that the southward extension of the fault is prepped for seismic activity. For stress change computations carried out with respect to receiver faults with strike 312°, dip 11°, and rake 127° at 15 km depth, the May 12, Mw 7.3 aftershock clearly falls within the region of high positive stress change (~4–6 bars), indicating that its rupture plane could have been optimally oriented to concentrate the imparted stresses (Fig. 4d). To further examine distribution of aftershocks in relation with the slip, we superposed them. The region of maximum slip, ~40 km southeast of the epicenter, corresponds to the region of lower aftershock productivity as compared to the eastern part, where the slip from the initial rupture was smaller (Fig. 5a). Slip from the May 12 event was highly localized around its source, with a tight clustering of aftershocks that grew SSE of maximum dislocation (Fig. 5b). Neither the low density of aftershocks in regions of maximum slip nor their growth outside the areas of maximum slip is unexpected, as observed for well-studied aftershock sequences globally (Das and Henry 2003).

Next we analyzed the distribution of aftershocks and slip along the 2-D geological cross sections, based on the tectonic and morphologic structure of central Nepal discussed in the literature. We took three transects (N1–N1′, K–K′, and N2–N2′) through the aftershock zone and the major structures including an out-of-sequence thrust (PT_2) theorized in the literature (Fig. 2). For all these profiles, we developed scaled depth sections, showing the down-dip projections of the major thrust faults, and hypocenters of aftershocks. From the section along N1–N1′, we note that the earthquake originated close to the down-dip trace of the southern margin of PT_2 (Fig. 6a). The E-W-oriented, 100-m-long surface deformation with nominal offset of ~10 cm falls south of this trace (Parameswaran et al. 2015). The InSAR data identify this region as the fringe zone demarcating coseismic uplift and subsidence (Lindsey et al. 2015). The computed slip right below this deformation zone is about 1.05–2.3 m.

Along the profile K–K′ the maximum slip of 2.9–3.525 m is observed below Kathmandu Valley, while the down-dip trace of PT_2 slipped 2.3–3.525 m (Fig. 6b). The third profile, N2–N2′ along the epicenter of the Mw 7.3 event, also suggests clear spatial association of the hypocenter with the down-dip trace of PT_2 (Fig. 6c). Almost all the aftershocks fall within the broad zone that represents out-of-sequence thrusting or regions to its south, with minimal numbers to the north. As for the southward projection of slip, it is evident that there was no transmission toward MFT, which explains why there were only minimal effects in the Gangetic Plains.

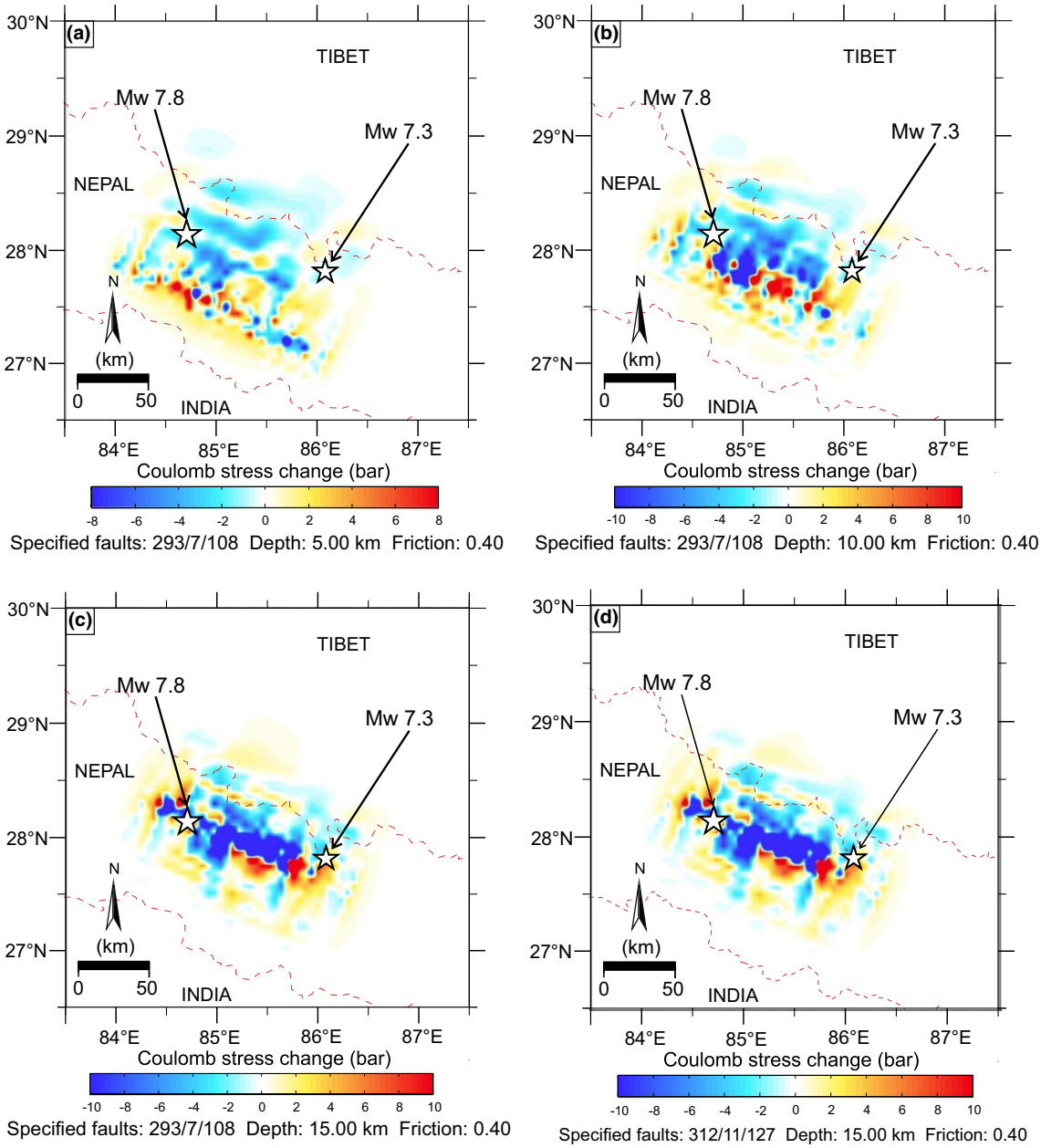

Fig. 4 Coulomb static stress change due to Mw 7.8 earthquake—with respect to the receiver planes of fault parameters identical to the parent fault (strike 293°, dip 7°, rake 108°) at **a** 5 km, **b** 7 km, **c** 10 km, **d** with respect to receiver faults with fault parameters of the Mw 7.3 event (strike 312°, dip 11°, rake 127°) at 15 km depth

Discussion

The 2015 pair of Nepal earthquakes is the first set of large earthquakes to have occurred in the central Himalaya during the post-broadband-GPS-InSAR period, providing an unparalleled opportunity to examine their rupture mechanisms vis-à-vis the prevailing understanding. It is generally believed that the great earthquakes in the Himalaya originate on the Main Himalayan Thrust (MHT), and their ruptures propagate to the Main Frontal Thrust (MFT). This idea is supported by reported coseismic effects of the great 1934 Bihar earthquake, reiterated by observations in shallow trenches in the foothills of the Himalaya. Ruptures originating on the MHT are also arrested by the mid-crustal ramp, leading to no surface deformation, as observed in the case of the 1991 Uttarkashi earthquake. On the other hand, earthquakes unrelated to the MHT tectonics are also known to generate surface rupture as evidenced by the 2005 Kashmir earthquake, which is believed to have originated on the IKSZ (Hussain and Yeats 2009). These observations

Table 1 Source model results for April 25, 2015, Nepal earthquake

Study	Method	Velocity model	Moment magnitude Mw	Rupture velocity V_r (km/s)	Rupture duration t_r (s)	Dip (°)	Maximum slip (m)
Avouac et al. (2015)	SAR imagery and backprojection model	IASP91	7.84	2.7–3.0	50	7	3–4
Fan and Shearer (2015)	Backprojection using teleseismic P-waves	IASP91	7.8	2.9	55	10	~4
Yagi and Okuwaki (2015)	Waveform inversion and hybrid backprojection model	CRUST 1.0	7.9	3.0	60	10	7.5
Hayes et al. (2015)	Finite fault modeling using teleseismic and geodetic data	CRUST 2.0	7.8	2.25	50	5–6	6
This study	Moment inversion using teleseismic P- and SH-waves	CRUST 2.0	7.85	2.75	50	7	4.175

suggest differing modes of rupture mechanisms for the Himalayan earthquakes, some reaching the surface either from MHT or from potential splay faults, and others arrested at the base of the ramp.

Our field investigations carried out soon after the 2015 events covering several locations including the Indian town of Gorakhpur did not reveal any evidence for significant ground shaking (such as venting of sand) until we reached the outskirts of Kathmandu (Parameswaran et al. 2015). It was clear that the April 25 earthquake showed yet another mode of rupture wherein the slip neither propagated to the MFT nor had any significant vertical component within its epicentral zone. Further, its eastward propagation was abruptly arrested at ~86°E, where a delayed, large aftershock occurred outside its immediate slip zone.

The large aftershock that occurred more than a fortnight later at the eastern terminus of the rupture area of the main shock is unusual in a region of continental collision and unprecedented based on the instrumental records in the Nepal Himalaya. Such an earthquake goes against the general notion that the spatial extent of aftershock activity of a given earthquake does not expand significantly after a week of the main shock (Das and Henry 2003). These authors also noted that clusters of aftershocks form at the edges of faults where there is an increase in static stress due to the large earthquake. Thus, ruptures of large aftershocks might overlap or abut one another at the edges but these are generally confined within the dimensions of the primary rupture zone. The May 12 event was sourced outside the zone of initial slip in a patch of high stress concentration, and its rupture was confined to a small area of 40 × 28 km^2. Most shocks that followed this later event occurred in a cluster within a source volume of 40 × 28 × 25 km^3. We note that the ruptures from both the earthquakes and their aftershock activities were abruptly arrested at ~86.5°E longitude, which marks the eastern limit of PT_2, suggesting a structural control in their spatial pattern.

It has been observed that aftershocks occur by slip on high stress patches left by the main shock rupture or by elastic stress transfer to the neighboring segments of the fault (Gomberg et al. 1998). Thus, with its own rupture dynamics and a series of spatially clustered shocks that followed, the Mw 7.3 earthquake that occurred a fortnight later qualifies to be called a triggered aftershock on the adjoining patch of stress heterogeneity. The size of this aftershock is also an important issue to be discussed. It has been argued that due to smaller size of the left over patches of stress concentrations, aftershocks within the initial rupture might be smaller, but a critically stressed adjacent strand might not be similarly constrained and thus could sustain similar size or larger aftershocks (Elst and Shaw 2015). The 2015 events provide the first modern-day example of such temporally and spatially paired large earthquakes in the Himalaya, whose sizes could potentially be controlled by the dimensions of the structural heterogeneities. Thus, it could be argued that based on the properties of the stress barrier, the size of an aftershock could be similar or larger than the previous earthquake. Such situations could have implications for post-earthquake hazard mitigation, and thus, there is a need for mapping the potential stress barriers in the study area.

Previous studies on the 2015 earthquake have suggested that the complex and multistage rupture could have resulted from multiple asperities, arrested by structural heterogeneities or rate-strengthening patches (Fan and Shearer 2015; Avouac et al. 2015). There are two aspects of these multiple ruptures that are worth discussing—one, the lack of southward relay of slip from both the earthquakes, and two, the

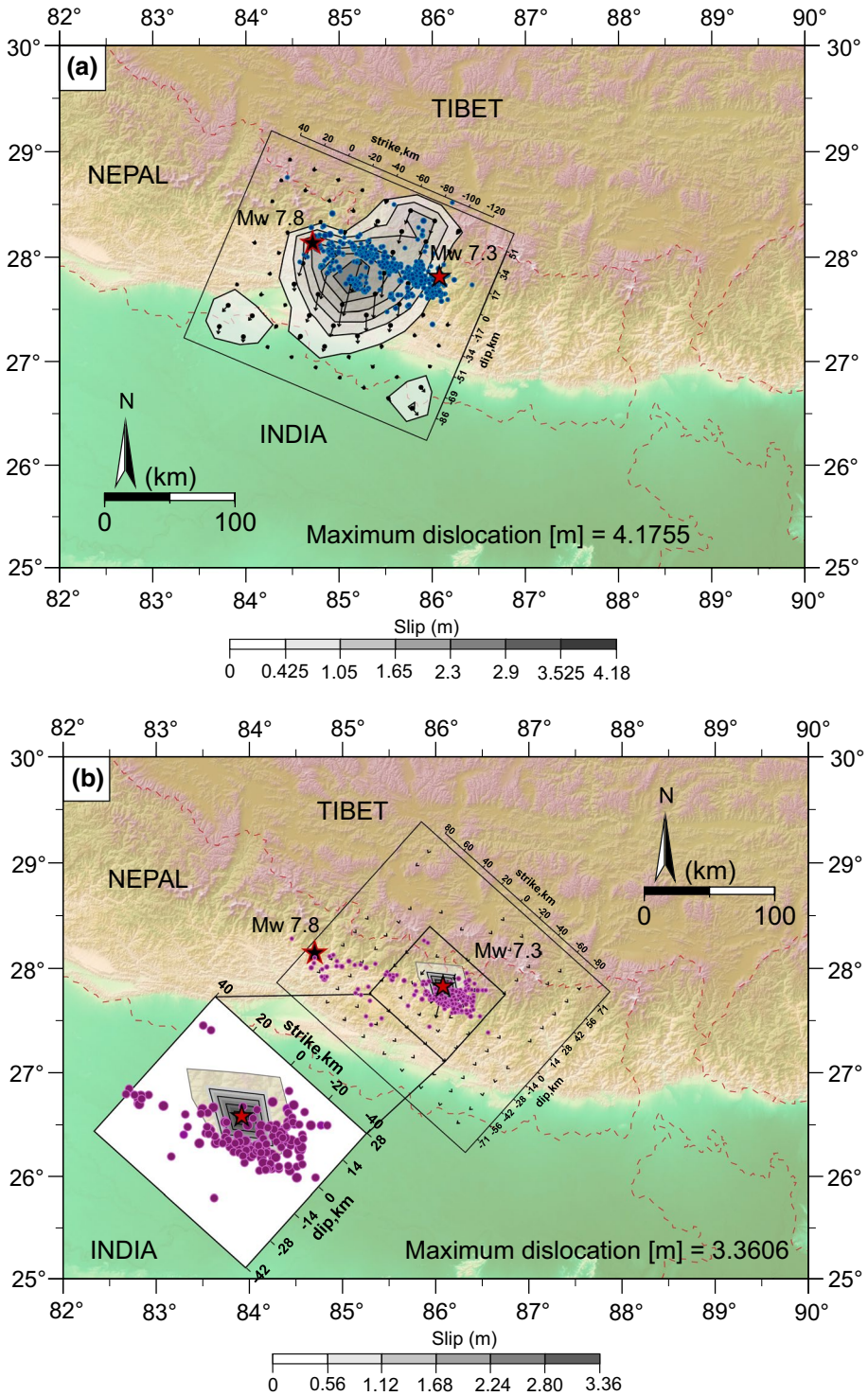

Fig. 5 **a** Slip distribution for the Mw 7.8 earthquake superposed with its aftershocks. **b** Same as (**a**) for the Mw 7.3 event; with the source region enlarged in the pop-out. Locations of the main events are plotted in both figures

abrupt termination of rupture from the second event. Our slip models and those by others (Avouac et al. 2015; Fan and Shearer 2015; Yagi and Okuwaki 2015; Hayes et al. 2015) suggest that the eastward propagating rupture was confined to the MHT and was arrested at around the same longitude (86.5°E) close to where PT_2 terminates, thereby making it one of the possible structural controls for the 2015 rupture propagation. The N–S transects across the slip area and aftershock zone suggest nominal slip (0–1.05 m) close to MBT and zero component along the MFT. The post-earthquake InSAR image validated this observation, and the maximum deformation was found to be colinear with what is believed to be PT_2. The potential subtle surface rupture that Parameswaran et al. (2015) reported at

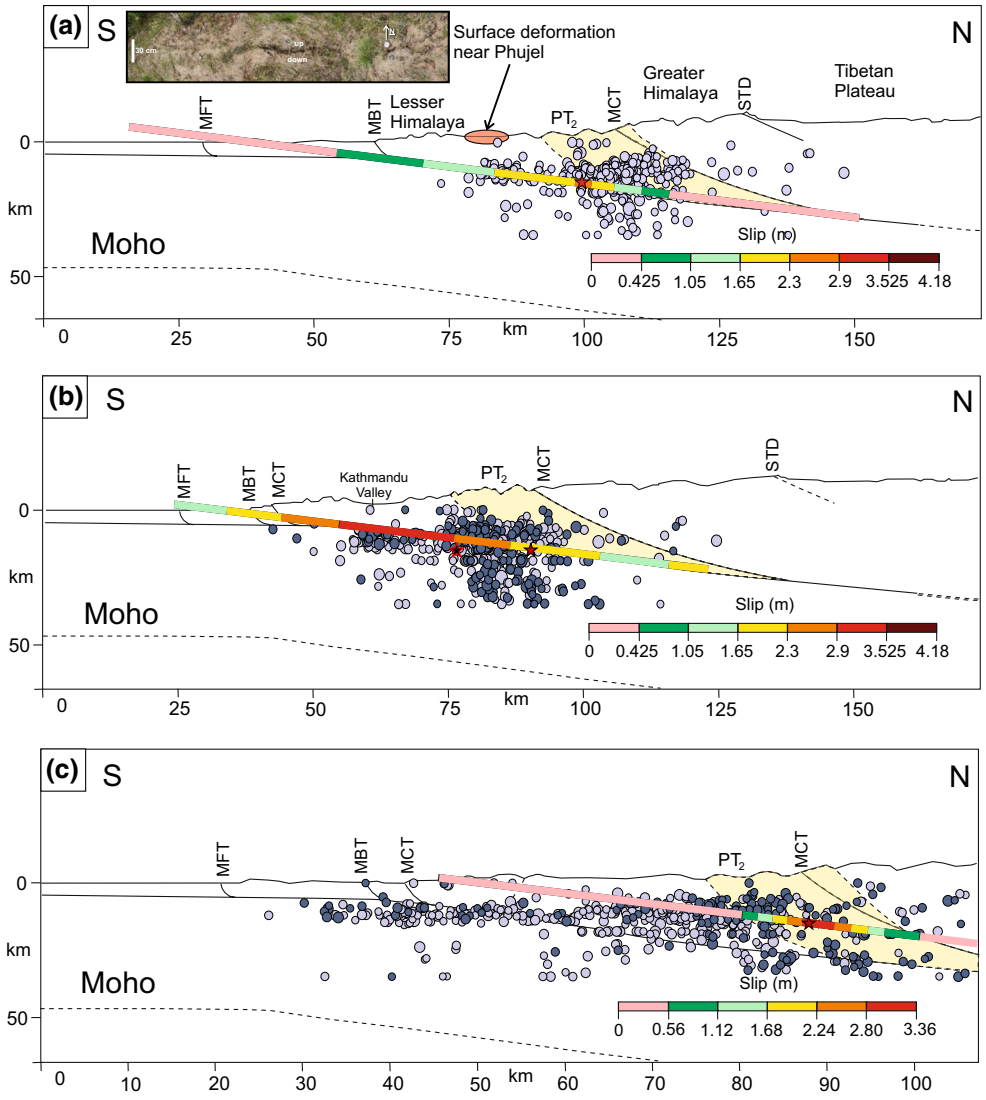

Fig. 6 Cross sections along profiles shown in Fig. 2. *Black* and *red stars* are the first and the second events, respectively. *Circles filled* in *lavender* are aftershocks between April 25–May 12 and those filled in *gray–blue* are post-May 12. Depths are scaled based on figures by Hodges et al. (2004), **a** section along N1–N1; *inset* shows one of the surface deformation features from Phujel, **b** section along K–K′, **c** section along N2–N2′. Location where surface deformation was observed by Parameswaran et al. (2015) is identified in (**a**). Modeled coseismic slips along the chosen profiles are shown using *various shades*

Phujel could have resulted from the up-dip propagation of slip, although the seismic slip model suggests that most of the slip was on the MHT. We believe that the termination of the initial rupture at ~86°E (Fig. 5a) and the development of the second pulse of activity, including the largest aftershock that terminated at 86.5°E, were controlled by out-of-sequence thrusting.

Our study also notes that since most of the slip got arrested ~50 km north of the MFT, the structural control could be either the Kathmandu klippe (although it does not extend to 86.5°E) or the out-of-sequence thrusting at PT_2. The up-dip portion of the rupture plane associated with the April 2015 event shows increased static stress change implying possibility for an impending activity in the region, or a possible aseismic slip. Although the latter poses little threat, a huge magnitude of damage can be expected in Nepal and Northern Indian if the region just north of the MFT slips. We observe the higher stress concentrations toward the eastern terminus of the rupture, which also shows higher aftershock activity and lower slip, implying the role of structural heterogeneity.

A schematic diagram showing the important structural features in the Nepal Himalaya (Fig. 7) summarizes the overall tectonic perspective. The segment pictured here between the Annapurna and Mt. Everest has been mapped as the extent of the out-of-sequence thrusting regarded as

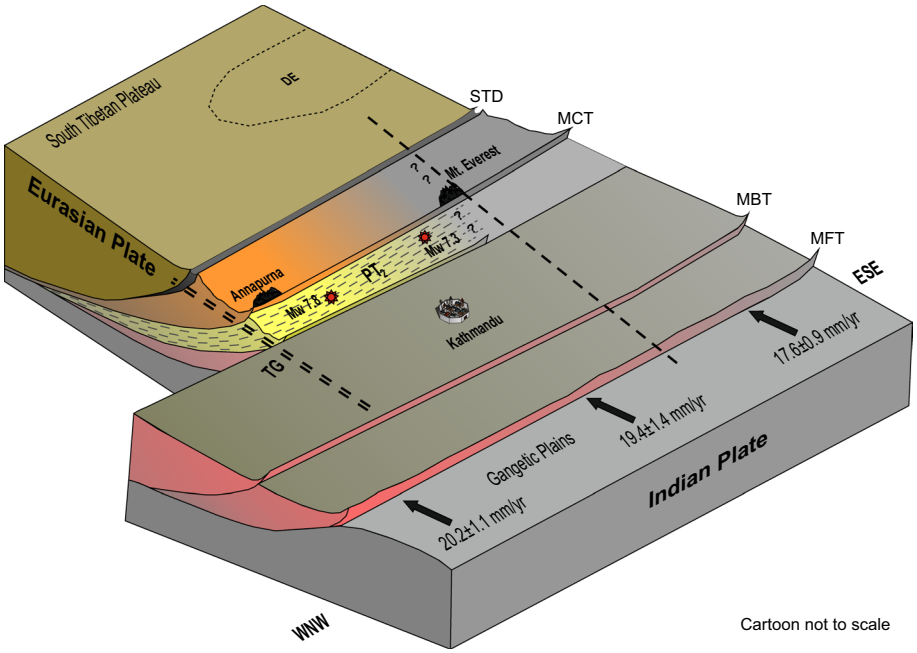

Fig. 7 Schematic diagram showing the tectonic setting of eastern Nepal region indicating major morphologic features, epicenters of the 2015 earthquakes, and important tectonic features. DE, marked similarly, is the zone of deeper extensional earthquakes (after de la Torre et al. 2007). *TG* Thakkhola graben. Note the eastward decrease in convergence rates

PT_2 (Wobus et al. 2005, 2006a, b). Recent GPS convergence rates suggest 19.4 ± 1.4 mm/yr along the segment between the Annapurna and the Thakkhola Graben (TG) (Figs. 1a, 7). Another important feature of this segment is the occurrence of deep-crustal and upper-mantle strike-slip earthquakes (de la Torre et al. 2007), mapped north of STD, possibly suggesting the activation on the leading edge of the Indian plate. Thus, from the physiography, GPS convergence rates, seismic productivity and velocity transitions, the eastern parts of the Nepal Himalaya between the Annapurna range and the Mt. Everest seem to be structurally quite distinctive.

The existence of PT_2 has been deliberated and debated as a significant out-of-sequence thrusting in the central Himalaya (e.g., Wobus et al. 2003), but there have been no specific references about its seismogenic potential. A similar physiographic transition has been observed in the Uttarakhand Himalaya (UPT_2) in the west, which is believed to have the potential to host large earthquakes (Morell et al. 2015). Based on this study, we suggest that the region between 84.5°E and 86.5°E stands out as morphologically distinctive, and its potential connection with large earthquakes needs to be explored. Although the 2015 earthquake was not sourced on PT_2, the structure may have played a role in accommodating part of the deformation. At this stage of the study, this is only a conjecture, but the role of physiographic transitions in accommodating convergence cannot be disregarded. Long-term monitoring using closely spaced GPS network could help in constraining the local deformation.

Conclusions

1. Earthquakes originating on the MHT are known for two modes of slip propagation, one that propagates all the way to the MFT, and the other where it is arrested at the mid-crustal ramp. The rupture mechanisms of the 2015 earthquake pair were different, wherein the ruptures neither reached the MFT nor did they produce any significant vertical slip at their sources. It appears that the 2015 pair presents a third mechanism whereby the rupture can be confined to the MHT, and part of the slip cold be accommodated by out-of-sequence splay thrust/s.
2. Given the rupture arrest ~50 km north of the MFT, a sizable amount of stress appears to be concentrated in the up-dip section of the April 2015 rupture plane. Unless it undergoes an aseismic slip, this region poses grave threat to Nepal and the Indo-Gangetic plains.
3. Many previous studies have invoked the existence of PT_2 as an important physiographic feature and an out-of-sequence thrust in the Nepal Himalaya, but none of them have considered the role of such structures in the seismogenesis of this region. This study for the first time relates the involvement of this structure in accommodating part of the slip, arresting the ruptures, and providing the structural control for a large aftershock and the events that followed.
4. Occurrence of a large aftershock immediately outside the initial rupture zone of a great/large earthquake has no known, modern precedents in the Nepal Himalaya.

The 2015 events offer an opportunity to study such a sequence. We conclude that the second large event was triggered on a contiguous patch of high stress concentration. Should such patches be larger than the initial rupture, the potential for a comparable or a larger size earthquake cannot be discounted, posing challenges in hazard mitigation. From this point of view also, the 2015 pair has important lessons to offer.

Data and resources

The Global Centroid Moment Tensor Project database was searched using www.globalcmt.org/CMTsearch.html to obtain the focal mechanisms of background seismicity. Seismograms for teleseismic inversion were obtained from the Incorporated Research Institutions for Seismology-Data Management Centre (IRIS-DMC) database. The aftershock data were obtained from the publication Adhikari et al. (2015). The subfault data for the Mw 7.8 event for Coulomb static stress change computation was obtained from the US Geological Survey (USGS).

Acknowledgments We acknowledge funding from the Ministry of Earth Sciences, Government of India, through project sanction MoES/P.O. (Seismo)/I(264)/2015 and the Indian Institute of Science, Bangalore, for conducting post-earthquake surveys in Nepal. The authors thank Prof. C.P. Rajendran for discussions and review of the manuscript and Prof. M. Santosh for suggestions to improve Fig. 7. RP thanks Prof. Hiroo Kanamori for discussions on the source models during various stages. We thank the reviewers Prof. Robert Yeats and Prof. Frank Roth for the insightful comments and suggestions that helped structure this paper better. We also thank Prof. Roland Burgmann, Prof. Douglas Dreger, Dr. Ruth Harris, Dr. Nicholas van der Elst, and Prof. Thorne Lay for comments on the poster version of this work at SSA 2016.

References

Ader T, Avouac JP, Liu-Zeng J, Lyon-Caen H, Bollinger L, Galetzka J, Genrich J, Thomas M, Chanard K, Sapkota SN, Rajaure S, Shrestha P, Ding L, Flouzat M (2012) Convergence rate across the Nepal Himalaya and interseismic coupling on the Main Himalayan Thrust: implications for seismic hazard. J Geophys Res Solid Earth 117:1–16. doi:10.1029/2011JB009071

Adhikari LB, Gautam UP, Koirala BP, Bhattarai M, Kandel T, Gupta RM, Timsina C, Maharjan N, Maharjan K, Dahal T, Hoste-Colomer R (2015) The aftershock sequence of the 2015 April 25 Gorkha–Nepal earthquake. Geophys J Int 203(3):2119–2124. doi:10.1093/gji/ggv412

Angster S, Fielding EJ, Wesnousky S, Pierce I, Chamlagain D, Gautam D, Upreti BN, Kumahara Y, Nakata T (2015) Field reconnaissance after the 25 April 2015 M 7.8 Gorkha Earthquake. Seismol Res Lett 86(6):1506–1513. doi:10.1785/0220150135

Armbruster J, Seeber L, Jacob KH (1978) The northwestern termination of the Himalayan mountain front: active tectonics from microearthquakes. J Geophys Res Solid Earth 83(B1):269–282. doi:10.1029/JB083iB01p00269

Armijo R, Tapponnier P, Han T (1989) Late cenozoic right-lateral strike-slip faulting in southern Tibet. J Geophys Res Solid Earth 94(B3):2787–2838. doi:10.1029/JB094iB03p02787

Avouac J-P, Meng L, Wei S, Wang T, Ampuero J-P (2015) Lower edge of locked Main Himalayan Thrust unzipped by the 2015 Gorkha earthquake. Nat Geosci. doi:10.1038/NGEO2518

Bassin C, Laske G, Masters G (2000) The current limits of resolution for surface wave tomography in North America. EOS Trans AGU 81:F897

Beaumont C, Jamieson RA, Nguyen MH, Lee B (2001) Himalayan tectonics explained by extrusion of a low-viscosity crustal channel coupled to focused surface denudation. Nature 414:738–742. doi:10.1038/414738a

Bettinelli P, Avouac JP, Flouzat M, Jouanne F, Bollinger L, Willis P, Chitrakar GR (2006) Plate motion of India and interseismic strain in the Nepal Himalaya from GPS and DORIS measurements. J. Geod. 80:567–589. doi:10.1007/s00190-006-0030-3

Bilham R, Gaur VK, Molnar P (2001) Himalayan seismic hazard. Science 293:1442–1444. doi:10.1126/science.1062584

Burbank DW, Blythe AE, Putkonen J, Pratt-Sitaula B, Gabet E, Oskin M, Barros A, Ojha TP (2003) Decoupling of erosion and precipitation in the Himalayas. Nature 426:652–655. doi:10.1038/nature02187

Cattin R, Avouac JP (2000) Modeling mountain building and the seismic cycle in the Himalaya of Nepal. J Geophys Res 105(B6):13389–13407. doi:10.1029/2000JB900032

Clark MK, Schoenbohm LM, Royden LH, Whipple KX, Burchfiel BC, Zhang X, Tang W, Wang E, Chen L (2004) Surface uplift, tectonics, and erosion of eastern Tibet from large-scale drainage patterns. Tectonics 23:1–21. doi:10.1029/2002TC001402

Cotton F, Campillo M, Deschamps A, Rastogi BK (1996) Rupture history and seismotectonics of the 1991 Uttarkashi, Himalaya earthquake. Tectonophysics 258(1):35–51. doi:10.1016/0040-1951(95)00154-9

Das S, Henry C (2003) Spatial relation between main earthquake slip and its aftershock distribution. Rev Geophys. doi:10.1029/2002RG000119

De la Torre TL, Monsalve G, Sheehan AF, Sapkota S, Wu F (2007) Earthquake processes of the Himalayan collision zone in eastern Nepal and the southern Tibetan Plateau. Geophys J Int 171:718–738. doi:10.1111/j.1365-246X.2007.03537.x

DeCelles PG, Robinson DM, Quade J, Ojha TP, Garzione CN, Copeland P, Upreti BN (2001) Himalayan fold-thrust belt in western Nepal. Tectonics 20:487–509. doi:10.1029/2000TC001226

Elst NJ, Shaw BE (2015) Larger aftershocks happen farther away: nonseparability of magnitude and spatial distributions of aftershocks. Geophys Res Lett 42(14):5771–5778. doi:10.1002/2015GL064734

Fan W, Shearer PM (2015) Detailed rupture imaging of the 25 April 2015 Nepal earthquake using teleseismic P waves. Geophys Res Lett 42(14):5744–5752. doi:10.1002/2015GL064587

Goda K, Kiyota T, Pokhrel RM, Chiaro G, Katagiri T, Sharma K, Wilkinson S (2015) The 2015 Gorkha Nepal earthquake: insights from earthquake damage survey. Front Built Environ 1:8. doi:10.3389/fbuil.2015.00008

Gomberg J, Beeler NM, Blanpied ML, Bodin P (1998) Earthquake triggering by transient and static deformations. J Geophys Res 103(B10):24–411. doi:10.1029/98JB01125

Grandin R, Vallée M, Satriano C, Lacassin R, Klinger Y, Simoes M, Bollinger L (2015) Rupture process of the Mw = 7.9 2015 Gorkha earthquake (Nepal): insights into Himalayan megathrust segmentation. Geophys Res Lett 42(20):8373–8382. doi:10.1002/2015GL066044

Hayes GP, Briggs RW, Barnhart WD, Yeck WL, McNamara DE, Wald DJ, Nealy JL, Benz HM, Gold RD, Jaiswal KS, Marano K (2015) Rapid characterization of the 2015 Mw 7.8 Gorkha,

Nepal, earthquake sequence and its seismotectonic context. Seismol Res Lett 86(6):1557–1567. doi:10.1785/0220150145
Henry C, Das S (2001) Aftershock zones of large shallow earthquakes: fault dimensions, aftershock area expansion and scaling relations. Geophys J Int 147:272–293. doi:10.1046/j.1365-246X.2001.00522.x
Herman F, Copeland P, Avouac JP, Bollinger L, Mahéo G, Le Fort P, Rai S, Foster D, Pêcher A, Stüwe K, Henry P (2010) Exhumation, crustal deformation, and thermal structure of the Nepal Himalaya derived from the inversion of thermochronological and thermobarometric data and modeling of the topography. J Geophys Res Solid Earth (1978–2012). doi:10.1029/2008JB006126
Hodges KV (2006) A synthesis of the channel flow-extrusion hypothesis as developed for the Himalayan-Tibetan orogenic system. Geol Soc Lond Spec Publ 268(1):71–90. doi:10.1144/GSL.SP.2006.268.01.04
Hodges KV, Parrish RR, Searle MP (1996) Tectonic evolution of the central Annapurna Range, Nepalese Himalayas. Tectonics 15(6):1264–1291. doi:10.1029/96TC01791
Hodges KV, Hurtado JM, Whipple KX (2001) Southward extrusion of Tibetan crust and its effect on Himalayan tectonics. Tectonics 20:799–809. doi:10.1029/2001TC001281
Hodges KV, Wobus C, Ruhl K, Schildgen T, Whipple K (2004) Quaternary deformation, river steepening, and heavy precipitation at the front of the Higher Himalayan ranges. Earth Planet Sci Lett 220:379–389. doi:10.1016/S0012-821X(04)00063-9
Hollister LS, Grujic D (2006) Pulsed channel flow in Bhutan; channel flow, ductile extrusion and exhumation in continental collision zones. Geol Soc Spec Publ 268:415–423. doi:10.1144/GSL.SP.2006.268.01.19
Hough SE, Roger B (2008) Site response of the Ganges basin inferred from re-evaluated macroseismic observations from the 1897 Shillong, 1905 Kangra, and 1934 Nepal earthquakes. J Earth Syst Sci 117(2):773–782. doi:10.1007/s12040-008-0068-0
Hussain A, Yeats RS (2009) Geological setting of the 8 October 2005 Kashmir earthquake. J Seismol 13(3):315–325. doi:10.1007/s10950-008-9101-7
Kaneda H, Nakata T, Tsutsumi H, Kondo H, Sugito N, Awata Y, Akhtar SS, Majid A, Khattak W, Awan AA, Yeats RS, Hussain A, Ashraf M, Wesnousky SG, Kausar AB (2008) Surface rupture of the 2005 Kashmir, Pakistan, earthquake and its active tectonic implications. Bull Seismol Soc Am 98(2):521–557. doi:10.1785/0120070073
Khattri KN (1987) Great earthquakes, seismicity gaps and potential for earthquakes along the Himalayan plate boundary. Tectonophysics 38:79–92. doi:10.1016/0040-1951(87)90067-9
Kikuchi M, Kanamori H (1991) Inversion of complex body waves-II. Bull Seismol Soc Am 81:2335–2350
Kikuchi M, Kanamori H (2003) Note on teleseismic body-wave inversion program, Earthquake Research Institute, Tokyo University, Japan. Online at http://www.eri.u-tokyo.ac.jp/ETAL/KIKUCHI
Lavé J, Avouac JP (2000) Active folding of fluvial terraces across the Siwaliks Hills, Himalayas of central Nepal. J Geophys Res 105:5735. doi:10.1029/1999JB900292
Le Fort P (1975) Himalayas: the collided range. Present knowledge of the continental arc. Am J Sci 275(1):44
Lindsey EO, Natsuaki R, Xu X, Shimada M, Hashimoto M, Melgar D, Sandwell DT (2015) Line-of-sight displacement from ALOS-2 interferometry: Mw 7.8 Gorkha Earthquake and Mw 7.3 aftershock. Geophys Res Lett 42(16):6655–6661. doi:10.1002/2015GL065385
Martin SS, Hough SE, Hung C (2015) Ground motions from the 2015 Mw 7.8 Gorkha, Nepal, earthquake constrained by a detailed assessment of macroseismic data. Seismol Res Lett 86(6):1524–1532. doi:10.1785/0220150138
Monsalve G, Sheehan A, Rowe C, Rajaure S (2008) Seismic structure of the crust and the upper mantle beneath the Himalayas: evidence for eclogitization of lower crustal rocks in the Indian plate. J Geophys Res Solid Earth 113:1–16. doi:10.1029/2007JB005424
Morell KD, Sandiford M, Rajendran CP, Rajendran K, Sanwal J (2015) Geomorphology reveals active décollement geometry in the central Himalayan seismic gap. Lithosphere 7(3):247–256. doi:10.1130/L407.1
Nábělek J, Hetényi G, Vergne J, Sapkota S, Kafle B, Jiang M, Su H, Chen J, Huang BS (2009) Underplating in the Himalaya-Tibet collision zone revealed by the Hi-CLIMB experiment. Science 325(5946):1371–1374. doi:10.1126/science.1167719
Pandey MR, Tandukar RP, Avouac JP, Vergne J, Héritier T (1999) Seismotectonics of the Nepal Himalaya from a local seismic network. J Asian Earth Sci 17:703–712. doi:10.1016/S1367-9120(99)00034-6
Parameswaran RM, Natarajan T, Rajendran K, Rajendran CP, Mallick R, Wood M, Lekhak HC (2015) Seismotectonics of the April–May 2015 Nepal earthquakes: an assessment based on the aftershock patterns, surface effects and deformational characteristics. J Asian Earth Sci 111:161–174. doi:10.1016/j.jseaes.2015.07.030
Rajendran K, Rajendran CP, Thulasiraman N, Andrews R, Sherpa N (2011) The 18 September 2011, North Sikkim earthquake. Curr Sci 101:1475–1479
Rajendran CP, John B, Rajendran K (2015) Medieval pulse of great earthquakes in the central Himalaya: viewing past activities on the frontal thrust. J Geophys Res Solid Earth. doi:10.1002/2014JB011015
Sapkota SN, Bollinger L, Klinger Y, Tapponnier P, Gaudemer Y, Tiwari D (2013) Primary surface ruptures of the great Himalayan earthquakes in 1934 and 1255. Nat Geosci 6(1):71–76. doi:10.1038/NGEO1669
Seeber L, JG Armbruster (1981) Great detachment earthquakes along the Himalayan arc and along-term forecasting. In: Simpson DW, Richards PG (eds) Earthquake prediction. American Geophysical Union, pp 259–277. doi: 10.1029/ME004p0259
Seeber L, Gornitz V (1983) River profiles along the Himalayan arc as indicators of active tectonics. Tectonophysics 92:335–367. doi:10.1016/0040-1951(83)90201-9
Stevens VL, Avouac JP (2015) Interseismic coupling on the main Himalayan thrust. Geophys Res Lett 42(14):5828–5837. doi:10.1002/2015GL064845
Wobus CW, Hodges KV, Whipple KX (2003) Has focused denudation sustained active thrusting at the Himalayan topographic front? Geology 31:861–864. doi:10.1130/G19730.1
Wobus C, Heimsath A, Whipple K, Hodges K (2005) Active out-of-sequence thrust faulting in the central Nepalese Himalaya. Nature 434:1008–1011. doi:10.1038/nature03499
Wobus C, Whipple KX, Kirby E, Snyder N, Johnson J, Spyropolou K, Crosby B, Sheehan D (2006a) Tectonics from topography: procedures, promise, and pitfalls. Geol Soc Am Spec Pap 398:55–74. doi:10.1130/2006.2398(04)
Wobus CW, Whipple KX, Hodges KV (2006b) Neotectonics of the central Nepalese Himalaya: constraints from geomorphology, detrital40Ar/39Ar thermochronology, and thermal modeling. Tectonics. doi:10.1029/2005TC001935
Yagi Y, Okuwaki R (2015) Integrated seismic source model of the 2015 Gorkha, Nepal, earthquake. Geophys Res Lett 42(15):6229–6235. doi:10.1002/2015GL064995
Yeats RS, Lillie RJ (1991) Contemporary tectonics of the Himalayan frontal fault system. Folds, blind thrusts and the 1905 Kangra earthquake. J Struct Geol 13:227–233. doi:10.1016/0191-8141(91)90068-T